Spring 5-21-2018

Association of p53 Polymorphisms, PAH-like Fluorescence, and Developmental Trends in Caught Gulf Menhaden to Crude Oil Exposure Post-Deepwater Horizon Oil Spill: A Holistic Approach

Kevin Luiz Frisina
kevin.frisina@student.shu.edu

Association of p53 Polymorphisms, PAH-like Fluorescence, and Developmental Trends in Caught Gulf Menhaden to Crude Oil Exposure Post-Deepwater Horizon Oil Spill: A Holistic Approach

Kevin Luiz Frisina

Acknowledgments

I would like to thank my former mentor Dr. Carolyn Bentivegna for introducing me to this project and for being a wholehearted guide throughout this research. She helped me further develop my passion toward the biological sciences in way that I had never anticipated. It was an honor to have worked with her.

In addition, I would like to thank Dr. Heping Zhou, and Dr. Liping Wei, for their guidance following Dr. Bentivegna's passing. They have shown great compassion and helped our research group during the chaos. They went above and beyond and for that we are thankful. Without your guidance, this work would have not possible.

I would also like to thank collaborators Samantha Reed and Dr. Wyatt Murphy for their invaluable assistance and input. Countless hours have gone into this project and together, and with their help, we got to where we are today.

Finally, I would like to thank my friends and family for their care and support throughout this process. During the many hours that went into lab and into writing this thesis, they motivated me to keep striving in spite of the hardships during this research.

Table of Contents

Abstract

Environmental pollution is of great concern in the United States. Of special concern is the chronic effects from the exposure to potentially carcinogenic compounds released from episodic environmental disasters (e.g. 911 twin-towers, oil spills). Disasters like the British Petroleum (BP) Deepwater Horizon oil spill in the Gulf of Mexico (GOM), affected many marine organisms, exposing them to crude oil polycyclic aromatic hydrocarbons (PAHs), some of which are known carcinogenic. Despite many marine-based consumer products (e.g. fish oil, animal feed, fertilizer) were known affected by the BP oil spill, bioaccumulation and chronic toxicity of the crude oil PAHs into marine organisms and overall wellbeing of marine organisms after the BP Deepwater Horizon oil spill are not fully understood.

In this study, Gulf Menhaden (*Brevoortia patronus*), one of the most important fish species in the consumer products named above, were studied. Wild Gulf Menhaden were caught from Vermilion Bay, Louisiana (VBLA) and Grand Isle, Louisiana (GILA) in 2012 and 2013. The menhaden were dissected and the tissue/organs were analyzed for crude oil PAHs via Excitation Emission Matrix Spectroscopy (EEMS) and 2D Fluorescence Spectroscopy. Genomic DNA was extracted from various fish tissue/organs, and was analyzed for polymorphisms in tumor suppressor gene *p53* DNA binding region (DBR) using PCR-SSCP (Polymerase Chain Reaction-Single Stranded Conformational Polymorphism) and in cloning-sequencing. The fish was also measured for body length and weight, which were used to evaluate its age and age-appropriate development.

PCR-SSCP results revealed polymorphisms of *p53* DBR in more than 50% of the menhaden individuals. The polymorphism was also tissue/organ dependent, and was greater in liver and gill than in muscle, heart or gonad. The DNA cloning/sequencing result suggested menhaden *p53* DBR diverged with low level of missense mutation in the exons and multiple

substations and insertion or deletion in the intron of *p53* DNA binding region which may affect gene splicing. The resulting *p53* variants may or may not be functional.

EEMS and 2D Fluorescence Spectroscopy scans revealed crude oil PAHs in all fish samples. The preliminary data suggest more crude oil PAHs (normalized to tissue/organ fresh weight) in the liver and gonad than gill, and that the low molecular weight PAHs were preferentially metabolized in all liver samples, with some showing more in-depth metabolism than the others.

Gulf Menhaden body length and weight did reveal developmental abnormalities and potentially abnormal single stranded *p53* DBR hairpins from cloning-sequencing within the given data. Additional work is needed to increase the sample size, which may further strengthen the preliminary observations in each of the three aspects of this study. Future work may further elucidate the functionality of P53 variants in Gulf Menhaden, and evaluate the long-term bioaccumulation and metabolism of crude oil PAHs to answer questions like “do the fish die prematurely from crude oil body burden, and what tolerances might Gulf Menhaden have to crude oil and crude oil derived PAHs?”

Introduction

On April 20th 2010, the wellhead of the Deepwater Horizon oil rig failed and unleased the largest maritime oil spill in the United States to date (Millemann, et al. 2015; Singleton, et al. 2016). The crude oil entered the ocean from 1500 meters under the surface, and then formed three distinct areas: a thin slick on ocean surface, an oil plume at 1100 meter below surface, and in sediment (Millemann, et al. 2015). Lighter polycyclic aromatic hydrocarbons (PAHs with 2 – 3 aromatic rings, e.g. methyl-naphthalene) are more common in the oil plume, while heavier PAHs (with 4 or more aromatic rings) such as fluorenes, phenanthrene anthracenes, and dibenzothiophenes, tend to persist in the surface slick and the sediment (Diercks, et al. 2010; Millemann, et al. 2015; Singleton, et al. 2016). Nearly 50% of the total released oil was dispersed by approximately 1.85 million gallons of dispersant, which increased PAH bioavailability in the water column up to 600 meters from the surface (Diercks, et al. 2010; Millemann, et al. 2015; Singleton, et al. 2016). PAH contamination from the crude oil is still a significant presence in the Gulf of Mexico years after the spill (Diercks, et al. 2010; Federal Interagency Solutions, 2010; Millemann, et al. 2015; Singleton, et al. 2016). Unfortunately, the scope of harm due to this spill is still not completely understood (Diercks, et al. 2010; Federal Interagency Solutions, 2010; Millemann, et al. 2015; Singleton, et al. 2016).

Major sources of PAHs in harbors and estuaries include incomplete combustion of gasoline, diesel, and oil, which increases especially under heavy boat traffic and oil spills (Bentivegna, et al. 2016; Pongpiachan, et al. 2017; Ramesh, et al. 2004;). PAHs are also in everyday products, such as in fireworks, and in grilled/smoked foods (Bentivegna, et al. 2016; Pongpiachan, et al. 2017; Ramesh, et al. 2004;). PAHs are believed to be formed mainly through a Diels-Alder slow condensation reaction (Llamas, et al. 2017; Shukla, et al. 2012). PAHs may also form via free

radical or ionic reaction mechanisms. Despite the extensive studies, the exact details of PAH formation preference and conditions are still uncertain (Llamas, et al. 2017; Shukla, et al. 2012).

PAH bioavailability across different environmental media must be considered (Bentivegna, et al. 2016; Pongpiachan, et al. 2017; Ramesh, et al. 2004). Certain PAHs may pass between media more easily than others, causing greater risk of exposure. Mackay model explains bioavailability in different environments (SETAC 1995). One of MacKay models suitable for marine oil spills shows the various fates of the crude oil (Farrington, 2014). According to Farrington (2014), PAHs from Deepwater Horizon oil spill are mostly bioavailable through sediment/soil and from the slick on the ocean surface, but they can also be available from the air and water (e.g. suspended or dissolved) (Farrington, 2014). In this spill model, the surface slick and ocean sediment would contain heavier PAHs (i.e. with 4 or more aromatic rings such as pyrene, fluoranthene and chrysene), and the water column would contain mostly two- or three-ringed compounds like naphthalene and anthracene, which has been confirmed by various studies (Farrington, 2014; Millemenn, et al. 2015; Ramesh, et al. 2004, Singleton, et al. 2016).

PAHs in crude oil in ocean oil spill are bioavailable upon dispersion or adsorption into organic material (Farrington, 2014; Millemenn, et al. 2015; Ramesh, et al. 2004). Dispersion, whether by natural weathering or artificial dispersant, is where the lipophilic crude oil gets dispersed into tiny droplets and thus the compounds within become more accessible and bioavailable (Farrington 2014; Federal Interagency Solutions 2010). This mechanism has been demonstrated by several studies to be responsible for PAH toxicity in fish, coral, bivalves and a variety of other organisms (Farrington, 2014; Millemenn, et al. 2015). Adsorption of PAHs into organic matter is also a concern due to their high partition coefficient (Saranjampour 2017). A partition coefficient (i.e. K_{OW}) describes how much of the substance (i.e. PAHs) would be present

in the unionized, fatty 1-octanol solvent phase when in equilibrium with the unionized aqueous solution (Saranjampour 2017). Since PAHs are highly lipophilic, they are easily taken up by organic materials (e.g. "marine snow" consisting of dead or dying microbes, animals, and/or sand), and/or are bioaccumulated in living organisms (Passow et al. 2016; Millemann, et al. 2015; Saranjampour 2017). Thus, PAHs in crude oil are bioavailable to organisms of the surface water as well as the deep water columns (Passow et al. 2016; Millemann, et al. 2015; (Saranjampour 2017).

PAHs enter the organisms, especially fish, through the gills or direct consumption of contaminated food. When PAHs diffuse through gills, they can then pass directly into blood circulation and exposing the vital organs immediately. If PAHs enter the organism from consumed a contaminated food (e.g. marine snow), the exposure may be slightly delayed (Ramesh, et al. 2004). Once in the organism, PAHs may accumulate in lipophilic tissues, or get oxidized by enzymes (e.g. epoxide hydrolase, mixed function oxidase, etc.) and may cause more toxicity (Mordukhovich, et al 2010; Ramesh, et al. 2004). Bioaccumulation and partial metabolism of PAH may cause significant dysfunction of the reproductive, immune, and endocrine systems. ATSDR (2009) illustrates the biotransformation of benzo(a)pyrene and possible effects of the metabolites in cells (ATSDR 2009; Bentivegna, et al. 2016; Pongpiachan, et al. 2014). Most notable among the detrimental effects is PAHs promoting carcinogenesis in fish as well as in humans (Bentivegna, et al. 2016; Mordukhovich, et al 2010; Ramesh, et al. 2004).

PAHs may be removed by some living organisms. One of the removing processes involves transmembrane proteins such as ATP-binding cassettes (i.e. ABC). In humans, ATP-binding cassettes protein would take certain GI (gastro-intestinal) absorbed PAHs and dump them back into the intestinal lumen (Ramesh, et al. 2004). Other removal processes would be through PAH

degradation. PAH degradation occurs mainly via the cytochrome P450 enzyme, which oxidizes hydrocarbons to epoxides. It was shown to occur in the liver, lungs, and kidneys in humans (Mordukhovich, et al 2010; Ramesh, et al. 2004). Next, the hydrolytic enzyme, such as the aryl-hydrocarbon hydrolase, would convert the epoxide into diols, which, with further modification, may be excreted, or undergo further modification and become a dihydrodiol epoxide (Mordukhovich, et al 2010; Ramesh, et al. 2004). The dihydrodiol epoxides can perform an S_{N1} or S_{N2} attack on the organism's DNA and cause gene damage (Mordukhovich, et al 2010; Ramesh, et al. 2004). PAHs, if not removed from the body by excretion, can form DNA adducts and introduce several point mutations, which may inactivate the gene or block DNA replication and gene transcription (Bentivegna, et al. 2016; Mordukhovich, et al 2010; Ramesh, et al. 2004).

In addition to removing PAHs from the body, an organism can also counteract on PAHs' carcinogenic effect by the activation of *p53*, an extensively studied tumor suppressor gene that serves as a biomarker for cancer (Lepre, et al. 2017; Uversky, et al. 2016). P53 protein suppresses tumors by causing the cells carrying unrepairable gene mutations to undergo apoptosis. When activated, the P53 DNA Binding Domain, along with appropriate transcription factors, associates to the specific erroneous gene sequence and promotes *p53* transcription (Lepre, et al. 2017; Uversky, et al. 2016). Increased *p53* transcription in cytoplasm triggers biochemical pathways leading to synthesis of caspase, which triggers apoptosis. The functional core region of P53 remains in active conformation and is conserved across species; both its Amino and Carboxyl Terminal Domains are species-specific and interact with various other regulatory proteins in order to assume active conformation (Lepre, et al. 2017; Uversky 2016). For example, under normal conditions, P53 is inhibited by regulatory protein Mdm2, which associates N-Terminal Domain of P53, blocking it in three ways: preventing transcription factors from associating to P53, promoting

ubiquitination of P53 (i.e. tagging P53 for proteasome degradation), and by exporting the P53-Mdm2 complex away from the nucleus via nuclear export signal on Mdm2 (Uversky 2016). When properly signaled, Mdm2 dissociates from the N-Terminal Domain which allows P53 to carry out its function. However, if mutation occurs to *p53* DNA binding region, it would result in P53's tumor suppressor function will be weakened (Lepre, et al. 2017; Uversky 2016). Such malfunction then prevents cells containing defective genes from being removed via apoptosis, and cells may accumulate additional gene mutations that may result in malignant tumors later on. In fact, *p53* was found mutated in 50-60% of all human tumors, with 97% of those mutations occurring in the core DNA binding region (Lepre, et al. 2017; Uversky, et al. 2016). Of these mutations, most of which are missense (Lepre, et al. 2017; Uversky, et al. 2016).

Gulf Menhaden (i.e. *Brevoortia patronus*) represents one of the ideal fish species to clarify the association between *p53* gene polymorphisms and the chronic exposure to environmentally relevant levels of PAHs from crude oil spills. Gulf Menhaden are generally estuarine, shallow water fishes. The juveniles and adults migrate offshore through summer and fall, spawn offshore during Sept to April. Such life cycle is typical of many estuarine fishes. Thus Gulf Menhaden had their spawning season and location coincided with the Deepwater Horizon oil spill. In addition, Menhaden's very high body fat content and filter feeding lifestyle (adult Gulf Menhaden filter approximately 2+ million gallons of water per year) make them easily susceptible to PAHs exposure from the oil spill (Bentivegna, et al. 2016; Millemenn, et al. 2015). More importantly, Gulf Menhaden are more genetically consistent across individuals than, for example, Atlantic Killifish, under normal conditions (Anderson, et al. 2014). These aspects of Gulf Menhaden would greatly help resolve the association of *p53* polymorphisms from PAH exposure.

Furthermore, Gulf Menhaden has economic relevance and are ecologically critical. Despite the Deepwater Horizon wellhead being declared sealed in September of 2010, it is suspected that much of that crude oil still persists and harms organisms, especially those living in the marshes and estuaries, including the developing Gulf Menhaden (Farrington, 2014; Millemenn, et al. 2015). This same area also holds the second largest fishery for Gulf Menhaden in the United States. If afflicted by the crude oil, Gulf Menhaden would negatively impact the fish bait, fish oil, and farm animal feed industries, as they are economic commodities derived mainly from menhaden (Bentivegna, et al. 2016; IUCN 2015; Millemenn, et al. 2015; Olson, et al. 2016). Aside from its economic relevance, Gulf Menhaden has critical ecological roles: they are filter feeders that consume phytoplankton, zooplankton and detritus, and are major prey for a variety of birds, fish, and mammals due to its high lipid content (IUCN 2015; Olson, et al. 2016). It serves as a major link between the producer and secondary consumers in the Louisiana bay area. If PAHs bio-accumulate in the fatty tissues of Gulf Menhaden, they may impact organisms in higher trophic levels, including human consumers (Bentivegna, et al. 2016; Millemenn, et al. 2015; Olson, et al. 2016).

Among the previous studies, Nadler and Bentivegna (2017) investigated the extents of phenotypic plasticity in Atlantic Killifish via force-feeding with crude oil. In their study, killifish were caught from Tuckerton, New Jersey, and after a two-week lab adjustment period, were separated into control and experimental groups (Nadler, Bentivegna 2017). The control group was administered 25 μL of 100% DayBrook's fish oil, while the experimental group was given 50% of fish oil from the same source and 50% of MC252 Deepwater Horizon crude oil prior to the 2010 spill (i.e. total volume also 25μL) (Nadler, Bentivegna 2017). Fish from both groups were then sampled at days 0, 1, 3 and 7 for weighing and length measurement (Nadler, Bentivegna 2017).

Liver and gallbladder samples of the fish were collected; the former (i.e. liver) was subjected to DNA extraction, where the core region of *p53* gene was amplified by PCR, cloned, sequenced, and run on the Single Stranded Conformational Polymorphism (SSCP) test; while the latter (i.e. gallbladder) was subject to fluorescence analysis for tissue PAHs qualification (Nadler, Bentivegna 2017). SSCP is important because it allows one to see single stranded mutations that would not otherwise be visible in agarose gel. In addition, Fluorescence Spectroscopy (either EEMS or 2D Fluorescence Intensity), allows one to visualize crude oil and crude oil derived PAH presence and metabolism (Bentivegna, et al 2016; Millemann. et al. 2015). Fluorescence scans showed that PAH-like compounds were present in the forced-fed killifish and that nucleotide level polymorphisms were detectable in SSCP test (Nadler, Bentivegna 2017). The connection between DNA polymorphisms and crude oil exposure still needs further investigation (Nadler, Bentivegna 2017).

This study is a collaborative work of myself and Samantha Reed, a graduate student with Dr. Bentivegna. We aim to examine Gulf Menhaden, as a representative fish species in Louisiana area to understand the impact of Deepwater Horizon oil spill on wild life at genetic level as well as in regard to holistic physical development. To achieve this understanding, we first confirmed the presence of PAHs-like compounds in wild caught Gulf Menhaden (Map 1 and 2), then determined polymorphisms in the *p53* DNA binding region. Custom PCR primers specific for Gulf Menhaden *p53* were designed from Atlantic Killifish *p53* DNA binding region sequencing data from Nadler's prior work (Nadler, Bentivegna 2017). The primer sets were tested using PCR on Gulf Menhaden's tissues, and were confirmed using agarose gel electrophoresis followed by cloning and sequencing. Part of the PCR products were run for SSCP test to find if insertion/deletions in the *p53* DNA binding region were present in the fish samples. Those same

amplified samples were also cloned and sequenced, where the results were then compared to each other and NCBI Blast data of Killifish *p53* DNA binding region to evaluate the polymorphisms. To determine PAH profiles, EEMS and 2D Fluorescence were measured and compared against fluorescence specific to PAH-like compounds in crude oil. Lastly, Gulf Menhaden fish weight and length data were plotted and compared to assess overall health and determine approximate age. It is hypothesized that the crude oil derived PAHs would be present in Gulf Menhaden, especially those from site of substantial oil spill, and its genome would contain polymorphisms in *p53* DNA binding region, and that weight vs length trend would be distorted.

Methods

Gulf Menhaden Collection Sites

Gulf Menhaden were caught from Vermilion Bay, Louisiana (i.e. VBLA) and Grand Isle, Louisiana (i.e. GILA), spanning 250 miles apart from both areas (Map 1 and 2) (Millemenn, et al. 2015). VBLA was set as the reference site because it was less affected by the crude oil based on oil transportation models, satellite imaging, and no shore oiling sites (Millemenn, et al. 2015). GILA, on the other hand, is the experimental site and was heavily polluted from the spill (Millemenn, et al. 2015). A standard 5-panel gill net approximately 200 meters long was used to collect menhaden during the summer of 2012 as well as the summer and fall of 2013 for both locations (Table 1). Fish from the same time and location are assumed to be part of the same school. The exact sampling locations for GILA Menhaden were as follows: 29°17′48.12″N 89°41′47.01″W; 29°15′58.27″N 89°56′34.31″W; and 29°10′ 35.74″N 90°3′41.34″W. VBLA fish, on the other hand, were caught in locations: 29°33′30.64″N 92°1′1.63″W; 29°34′54.00″N 92°5′36.00″W; and 29°28′20.93″N 91°49′57.77″W.

Fish Samples, DNA Isolation & Quality/Quantity Assessment

Caught Gulf Menhaden were stored in a -20°C freezer after capture. Prior to dissection, all fish had their fork length and weight recorded (Table 1), where this data was then used to correlate height vs weight trends for both VBLA and GILA fish (Figure 7). Organs or tissues were dissected from fish for DNA isolation (Table 1). The DNA from the selected tissues were extracted using Invitrogen DNAzol® reagent according to the standard protocol. Only modification was that the final solutions were in sterile x1 TE solution (i.e. 10 mM Tris, 1mM EDTA pH 7.8) to prevent enzymatic degradation of isolated DNA. The isolated DNA samples were checked using a UV-

Vis spectrophotometer (Nanodrop, Thermofisher) for DNA quality and quantity. DNA samples were then buffered with 23.17 µL of 0.1M HEPES to pH 7.8 (i.e. applied to the remaining 198µL of DNA isolate, as 2 µL of isolate was used in Nanodrop) and treated with 1µL of EDTA. Data on DNA concentration was adjusted to reflect these adjustments.

PCR, Agarose Gel Electrophoresis, and SSCP

p53 DNA binding region from the fish samples were amplified using PCR with custom-designed *p53* forward and reverse primers. (i.e. names F4 and R0 respectively). The primers were designed from sequencing results of Atlantic Killifish p53 DNA binding region (Nadler, 2017), based on cross-species conservation. The primers were designed using OligoAnalyzer 3.1 (IDT DNA); each one was to be 20bp long, and each set would have no or low spontaneous hetero/homodimerization and have similar annealing temperatures. PCR program was as following: 3 set for three minutes at 95°C, then cycle 45 times in segments of 95°C, 60°C, and 72°C (a minute each). Final reannealing segment run for three minutes at 72°C prior to being placed at a 4°C hold. PCR products were then stored in a -4°C freezer. A 2% agarose gel electrophoresis of the PCR products were run, along with 100 bp DNA ladder. Proportionally equal amount of dye were used for all agarose gel electrophoresis (i.e. 1µL of Ethidium Bromide per 25mL of 2% agarose solution).

Once the PCR products were confirmed by the agarose gel electrophoresis, the PCR samples were tested for Single Stranded Conformational Polymorphisms (SSCPs). We used Mini-PROTEAN® 10% TBE Urea Precast Gels (Bio-Rad), and the gel was placed in the middle alignment slot of the mold. 0.5x TBE filled in both the inner and outer compartments, thereby bathing the gel in buffer. The apparatus was set on ice, and was pre-run in 0.5X TBE for 1 hour

at 200 volts. Then, 6 µL of PCR product was mixed with 12 µL of formamide dye loading buffer (Invitrogen, Vilinius, LI) and the mixture was heated 95ºC for 10 minutes to separate the DNA into single strands. The sample mixtures were then incubated on ice for 10 minutes and was loaded into gel wells with 100 base RNA Ladder (RNA Century Size Marker P/N: AM7140). The gel was then run at 72 volts for 3 hours while on ice. Once the tracking dye ran to the bottom of the cast, the gel was opened, removed, and immersed in 500 mL of 10% acetic acid (v/v), covered and set on an oscillatory shaker for an hour. The acetic acid was subsequently decanted and was replaced with 500 mL of distilled water, where the gel was again covered and shaken for another 20 minutes or until the tracking dye was no longer visible on the gel. The water was then decanted and gel was then stained with 1x SYBR Gold Nucleic Acid Gel stain (Invitrogen, S11494, prepared via adding 5µL of 10,000 stain to 50 mL of deionized water). The gel was then promptly covered and placed back onto the oscillator for another 30 minutes. The gel was then removed and viewed on a UV transilluminator (Proteinsimple, Santa Clara, CA, USA) to visualize the band pattern of the single stranded DNA.

Cloning and Sequencing

The PCR products from one each of VBLA and GILA fish were cloned following the protocol provided in the TOPO® TA CLONING Kit (Invitrogen, Ref number45-0641). Using M13 forward primer specific for the plasmid vector and the *p53* specific R0 reverse primer, the positive clones were run on PCR and the PCR products were sequenced (GenScript DNA Sequencing Service, GenScript Biotech, NJ). The nucleotide sequencing data was then converted into equivalent amino acids and compared to both Atlantic Killifish and themselves in order to determine the effects of translated polymorphisms onto P53.

PAH Extraction, PAH Standards and Reagents, EEMS and 2D Fluorescence Analysis

PAHs from 0.05 g fish organs or tissues were extracted into 75% ethanol upon homogenization and were further diluted by 10-fold in 75% ethanol before fluorescence analysis. Crude oil samples from MC252 crude oil were also prepared in 90%, 75% and 50% ethanol for fluorescence analysis, which was prepared by taking 12.5 microliters of 100% MC252 Crude oil (used just prior to the Deepwater Horizon oil spill) and diluting it with 999.75 microliters of 75% ETOH (i.e. to have a final crude oil concentration of 1.25% by v/v). The diluted crude oil solution was scanned with the Horiba (i.e. for 3D EEMS).

The fish samples and crude oil samples were analyzed on Horiba Fluorlog®4 (model FL-1000, Horiba Jobin–Yvon, Edison, NJ) using FluorEssence software (V3.5) and SpectraMax® M5/M5 (Catalog Number: 89212-398). The Horiba Fluorlog®4 generates a 3-D contour map, while the SpectraMax® M5/M5 develops fluorescence intensity vs excitation wavelength graphs at a set emission wavelength. It was set with excitation wavelength of 260-400 nm and recording the emission at wavelength of 320-480 nm. The fluorescence were represented in photon counts per second per microamps (CPS/ μAmp). 2D fluorescence profile of the fish samples were obtained at 440 nm emission and an excitation of 260- 400nm, with fluorescence intensity of 0 – 90,000 counts CPS/ μAmp. 3D fluorescence contour maps and 2D profiles may help characterizing the PAHs-like compounds in the fish samples.

Results and Discussion

Primer Set for Gulf Menhaden p53 DNA binding region

NCBI refernece sequence for Atlantic Killifish *Fundulus heteroclitus p53* transcript variant X1 was shown in Fig. 1A. Its DNA binding region approximately starts at around 760 and ends at 960 nt; it contains two exons, each of about 100 bp and showing high alignment scores different fish species (Fig. 1B, pink areas). One intron of about 167 bp was shown in cross-species alignment with low alignment scores (Fig. 1B black areas, the intron does not appear in the transcript sequence in Fig. 1A).

Primers were designed from *F. heterolitus p53* transcript sequence. Three forward (F1, F3, and F4) and four reverse primers (R0, R1, R2 and R3) were designed. Nucleotide position 601 was where F3 primer started, 768 the start of F4 (Fig. 1A highlighted), F1 was 7 nt upperstream of F4; R0 was from 946 – 965 nt, R1 was 20 nt upsteam of R0, and R2 4 nt downsteam of R1, and R3 was most upstream and from 878 – 897 nt.

The probable homo- and hetero-dimers and the corresponding Gibbs free energy were shown in Fig. 2 A – C for F4, F3 and F1 pairing with each of the four reverse primers respectively. Fig. 3E tabulated Gibbs free energy of the homo- and hetero-dimers. The primer sequences and melting temperatures were shown in Fig. 2D. Typically the less negative Gibbs free energy, the less likely for spontaneous dimerization.

F1 with R1, R2 and R3 were tried first. While a single band of about 300 – 350 bp was expected, these primer sets produced multiple bands of no more than 200 bp (Fig. 3C) from menhaden genomic DNA samples. Thus F1 primer was not ideal. Next, F3 with R2 was tried. A single band about 520 bp was expected, but the result was, for most samples, a wide band of about 50 bp, probably just primer dimers or other PCR artifacts, except in one sample there was

a band at 250 bp (Fig. 3B, right side of the ladder). Since R2 and R1 were very similar, F3/R1 was not tried after the failure of F3/R2.

Lastly, F4 was tried with R1 and R0, expecting single band of about 340 and 360 bp respectively. F4/R1 resulted in single band around 150 bp (Fig. 3B, left side of the ladder) thus was decided not working. Luckily, F4/R0 generated single sharp single bands at expected size of 360 bp for various menhaden's genomic DNA samples (Fig. 3A). Further tests found F4/R0 consistently worked with additional menhaden's genomic DNA samples. Other primer sets were not tried once F4/R0 was found robust and successfully.

It is intersting to note that among the primer pairs tested, F4 produced mostly single bands with R1, although of unexpected size (i.e. 150 bp instead of 340 bp). The PCR product was later cloned/sequenced and was found to contain the first exon and portion of the intron of *p53* DNA binding region. Such truncation suggests tat the reverse primer R1 was not functional in PCR. It is possible that the single stranded DNA with 1st exon and part of the intron formed hairpin loops (Fig. 9B and L) allowing its amplification during PCR but had to be truncated without the aid of a functional reverse primer (Figure 9 B and L; Yeo, et al. 2016).

Figure 1. Determination of Menhaden P53 DNA Binding Region and P53 DNA Binding Region Features

Figure 1: Figure 1A from NCBI BLAST service represents the original DNA Binding region provided from Allison's Atlantic Killifish work, which Figure 1A is presenting the DNA equivalent of the transcribed *p53 DBR* mRNA. The highlighted sequence on lines 601 and 661 are the sequence for Forward primers F3 (i.e. line 601), F1 and F4 (i.e. both on line 721). Line 841 contains the whole R3 reverse primer, highlighted in yellow in addition to the ending and beginning part of exons 1 and 2 respectively. Line 901 contains R1, R2 and a portion of R0, which they are indicated using boxes. The highlighted portion of line 961 represents the approximate end of the DNA Binding region as well as the end of the R0 reverse primer. Figure 1B represents the generic conserved sequence locations in pink on *P53*, which the 1st exon is on the left and the 2nd exon is on the right. The species-specific intron spans between the two exons and is represented as a black line. This intron is absent in the Killifish mRNA in Figure 1A.

Figure 2. Custom Menhaden P53 Primer Set Development

Dimerization Predictions

Custom Primer Sequences

Spontaneity of Dimerization for F1, F4 and F3 primers to R0, R1, and R2,

Expected P53 DNA Binding Region Template Sizes According to Selected Primer Set

Figure 2: Based off the Killifish *P53*, Custom Forward and Reverse primers were designed to be 20bp long and not have spontaneous dimerization with the selected set. Using the OligoAnalyzer 3.1 service from IDT DNA, Figures 2A-C and E were generated. Figures 2A-C show homo/heterodimerization trends of Forward Primers, F1, F3, and F4 toward reverse primers R0, R2, and R3. Figure 2D-F were primer annealing temperatures, spontaneity of homo/heterodimerization trends in tested primer sets and expected P53 DNA Binding Region Template Sizes according to selected primer set as provided by Genescript's DNA Sequencing service.

Figure 3. Primer Set Testing

Figure 3: These gels were done in 2% agarose, 0.5x TBE buffer and dyed with 4μL of 10 mg/mL Ethidium Bromide in order to test the functionality of our proposed primers. Figure 2A shows forward primer F4 with R0 in all samples. The gel on Figure 3B consisted of two possible forward primers (i.e. F3 & F4) and three possible reverse primers (i.e. R1 & R2). Figure 2C shows primer testing of F1 forward primer with R1, R2, and R3 reverse primers. A primer set was considered successful if it generated a sharp band approximately equal to the expected size of P53 DNA binding region template (Figure 2F). All gels use a DNA100bp ladder. Only F4 and R0 best fit this description (Figure 3B).

PCR-SSCP with F4/R0 DNA Profiles

Since SSCP was done with 10% TBE-Urea denaturing gels and sensitive Sybergold DNA stain, we expect that any deletion and insertion mutations would show up as SSCP band(s) of a size other than 360 bases (that is, one band of 360 bases was expected at normal conditions). The lanes on SSCP gel were labled for fish samples e.g. GILA 562 L is liver sample from fish 562 collected from GILA; M, L, G, H, D represnts muscle, liver, gill, heart and gonads respectively. Fish ID number can be cross-referenced with Table 1 and Map 1 and 2 for collection date and site locations.

Among all the fish samples analyzed, 22 samples from 11 individuals showed sharp bands and clear patterns (Fig. 4 A, C, D, and B-the 2nd lane from left), and 15 samples from 8 individuals had fuzzy but identifiable bands (Fig. 4 B, E-G).

PCR-SSCP showed three band patterns: one band of about 360 bases (pattern I), e.g. GILA 556H, two-band of ~ 360 and 200 bases (pattern II, e.g. 278M), and three-band of ~ 360, 200 and 100 bases (pattern III, e.g GILA 562L). We compared number of fish and samples (and organs specific samples) showing different patterns (Fig. 4H). Because the patterns seemed to be dependent on organs and the organ that were sampled were not even between VBLA and GILA fish, we could not compare VBLA and GILA samples directly. The pattern distribution is as following:

1) Equal number of fish showed pattern I and II (9 fish, 47% each), and only one fish with pattern III (5%)
2) More samples showed pattern II (20 samples, 54%) than pattern I (16 samples, 43%) than pattern III (1 sample, 3%)
3) Liver and gill samples did not have pattern I, but were predominatly with patter II (88%, 100% for liver and gill respectively). One liver sample had pattern III (12%).

4) 83% gonad samples, 62% muscle samples, 60% heart samples showed pattern I, with the remaining of pattern II.

It suggests that nearly half of the fish had *p53* polymorphisms; most with two but 5% with three forms. Polymorphism was substantially greater in liver and gill than in skeletal muscle or heart. Gonad was most conserved with only 17% samples showing polymorphism. This seems to be consistent with exposure and function of organs, e.g. liver metabolizes PAHs from crude oil exposing it directly to more carcinogenc PAH metabolites; gills are directly exposed to PAHs because of menhaden's filter feeding behavior; and gonads may be evolutionarily protected from *p53* polymorphism so that the offspring may be normal and the species would continue and survive. On the other hand, the small sample number in this study may cause certain bias in certain percentages, but the qualitative trends would likely hold. Future work should increase sample number to derive more robust conclusion on *p53* polymorphisms in Gulf Menhaden.

Table 1. GILA and VBLA Fish Collection Data

Coastline Area	Date Collected	Samples	Tissues	Fish Weight (g)	Fish Length (cm)
VBLA	8/16/2013	270	L	131.0	18.5
		271	LM	135.0	19.0
		272	MD	194.0	21.5
		273	*	166	19.5
		274	*	117	17.5
		275	*	181	20.5
		276	GLMH	137.0	19.5
		277	G	132.0	18.0
		278	MGLH	154.0	18.5
		279	MDH	195.0	21.5

Coastline Area	Date Collected	Samples	Tissues	Fish Weight (g)	Fish Length (cm)
VBLA	6/8/2013	291	GLMH	168.0	19.0
		292	*	87	16.4
		293	*	126	16.6
		294	*	77	17.6
		295	GLMH	112.0	18.0
		296	*	132	17.3
		297	*	167	20.2
		298	*	139	17.1
		300	L	197.0	19.5
		301	*	250	22.5
		302	LM	189.0	19.5
		303	*	138	17.9
		304	*	163	19.5
		306	*	218	21.5
		309	*	167	20.1

Coastline Area	Date Collected	Samples	Tissues	Fish Weight (g)	Fish Length (cm)
GILA	9/11/12	410	G, L	137.0	19.0
		413	D	152.0	18.3
		422	L	105.6	17.7
		423	L	94.3	16.4

Coastline Area	Date Collected	Samples	Tissues	Fish Weight (g)	Fish Length (cm)
GILA	9/10/2013	510	*	96	16
		511	*	109	17
		512	*	119	17.5
		513	*	98	17.6
		514	*	108	18
		515	*	104	20.5
		516	*	90	16.4

Coastline Area	Date Collected	Samples	Tissues	Fish Weight (g)	Fish Length (cm)
GILA	6/20/13	520	L	64.0	15.2
		521	M	55.0	14.8
		522	*	69	17.4
		523	*	63	14.9
		524	*	65	16.8
		525	*	64	16.6
		526	*	51	15.8
		527	L	61.0	16.8
		530	L	53.0	13.7
		531	L	53.0	137
		532	LM	58.0	17.3
		533	LM	68.0	15.6
		534	LM	55.0	16.8

Coastline Area	Date Collected	Samples	Tissues	Fish Weight (g)	Fish Length (cm)
GILA	8/19/13	550	*	41	13.1
		551	*	50	13
		552	*	43	14.7
		554	L,G	50.0	15.0
		556	H	43.5	13.0
		558	*	45	12.7
		559	*	41	13
		560	M	46.0	15.1
		561	*	32	12.5
		562	LM	31.0	11.5
		563	*	40	14.8
		564	L	36.0	12.2
		565	*	41	13.1
		566	*	45	15.5
		568	*	36	12
		569	*	38	12.5

Table 1: All menhaden fish were caught at either Vermillion Bay or Grand Isle and were numbered accordingly. Fish were frozen at -4°C and had measurements (i.e. Mass and length) taken prior to dissection. Measurements used to determine the approximate age of the fish in relation to one another are presented for each fish in these graphs. Charts are separated by season and location (i.e. VBLA or GILA). Each fish was given a unique number. Tissues L, G, M, H, and D correspond to Liver, Gill, Skeletal Muscle, Heart, and Gonad respectively.

Map 1. Louisiana Gulf Menhaden Collection Site Map and Oil Spill Maps

Louisiana Gulf Menhaden Collection Site Map

Map 1: Courtesy of Alexrk2 who produced this image, which has been edited from the original to show where the Gulf Menhaden were caught in VBLA (i.e. blue star) and GILA (i.e. orange star) locations during 2012 and 2013. In no way does the original creator of this image endorse any finding in this thesis, as this map is only used for illustrative purposes. URL: https://commons.wikimedia.org/wiki/File:USA_Louisiana_location_map.svg

Map 2. Deepwater Horizon Oil Spill Spread Map

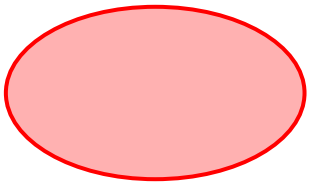

Map 2: Courtesy of the U.S. National Oceanic and Atmospheric Administration, who produced this image, which has been edited from the original image to show where Gulf Menhaden were caught in VBLA (i.e. blue star) and GILA (i.e. orange star) and the approximate afflicted area of the crude oil spill as of September 2010. The approximate wellhead location is indicated by a yellow star. This image does not represent the later spreading of crude oil into the Gulf of Mexico in later years. In no way does the original creator of this image endorse any finding in this thesis, as this map is only used for illustrative purposes. URL: https://commons.wikimedia.org/wiki/File:GulfofMexico3D.jpg

Figure 4. PCR-SSCP with F4 R0 Primer Set

Figure 4: All gels were done in 10% TBE-Urea denaturing gels (Mini-Protean Precast Gel BIORAD; Catalog Number 4566036) and 1x Sybergold (Catalog Number S11494) in order to observe deletion and insertion mutations present in the selected menhaden tissue samples. All gels use a 100bp RNA ladder (RNA Century Size Marker; P/N AM7140). Samples did show the expected 360bp band, but many samples displayed an unexpected second band (e.g. VBLA 279 D,L & GILA 526M), at about 200bp. Interestingly, sample GILA 562L (Figure 4B) displayed multiple bands (one 360bp band, one 200bp band, and one 100bp band). Some samples also only display one band (Figure 4G) (i.e. 560M & 521M [GILA]; 279MH, 276M, 271M [VBLA]). Banding pattern trends are displayed in Figure 4H. All previously recorded trends were listed as Pattern 1 (i.e. 1 SSCP band), Pattern 2 (i.e. 2 SSCP band), or Pattern 3 (i.e. 3 SSCP band).

3D Excitation Emission Spectroscopy and 2D Fluorescence Scan Results

The purpose of 3D and 2D fluorescence analysis was to determine the presence of PAHs like compounds in the fish samples and to compare GILA and VBLA fish tissue PAHs (Figure 5 and 6).

The PAHs in the crude oil samples (1.25% crude oil in 50%, 75% or 90% ethanol) generated strong fluorescence signals (0.5 – 2.5 x 10^7 CPS/µA; Fig. 5A – C). The EEMS fluorescence center (the high intensity area) of the contour maps shifted up- and right-ward (longer excitation and emission wavelengths) when the solvent ethanol increased from 50%, 75% to 90%. Both 75% and 90% ethanol would produce fluorescence contour map for PAHs relatively free from interference due to biomolecules in fish tissue e.g. albumin, which fluoresced in lower left corner (excitation: 260 – 300 nm, emission: 320 – 400 nm, as was observed in Nadler's control fish gall bladder samples), and vitamin A, which fluoresced at mid-right edge area (ex: 310 - 340 nm, em: 450 - 480 nm, with 1 – 1.5 x 10^5 CPS/µA fluorescence intensity at 100,000 ng/mL in 75% ethanol, Pena et al., 2015) (Figure 5B Circled). We chose 75% ethanol as solvent for its ability to differentiate crude oil PAH fluorescence from fish biomolecules' fluorescence and to minimally sacrifice fluorescence resolution for PAHs (a very nice comparison of EEMS of fluorescent biomolecules and that of crude oil appeared in Bentivegna et al., 2016, which further supported the choice of 75% ethanol).

Two contour peaks were also observed and compared to the stared regions in Figure 5B. Contour peak 1 (Figure 5A-J) representing larger molecular weight crude oil-derived PAHs with more aromatic rings. Contour Peak 2 (Figure 5G, I, and J) corresponded to lower molecular weight PAHs with fewer aromatic rings. These contour peaks seem to shift in certain samples. For example, the center of the contour map in fish liver or gonad sample (Fig. 5D - E) shifted up- and right-ward (longer wavelength). This may suggest that the liver and gonad tissue

preferentially retained higher molecular weight (HMW) PAHs than the low molecular weight (LMW) PAHs. This may be due to more rapid enzymatic metabolism of LMW PAHs by liver. It is also interesting to notice that the gill sample (Fig. 5E), though of lowest fluorescence among the fish organs examined, seemed to have a contour map center shifted rightward only as compared to the crude oil sample. This may suggests that limited metabolism in the gill as compared to in the liver or gonad, which seems consistent with the menhaden's filter feeding behavior thus gill would be among organs that directly contact PAHs in crude oil.

EEMS for menhaden samples were shown in Fig. 5D – J. It is remarkable that all fish samples showed the presence of crude oil fluorescence in the order of 10^5 CPS/μA. When different organs from the same menhaden (GILA420) were compared, fluorescence intensity was higher in liver sample than the gonad, which was higher than the gill sample (Fig. 5D – E). This result was also found in the 2D Fluorescence scans (Figure 6).

Due to confirmation of PAH accumulation in the liver, additional GILA and VBLA liver samples were studied. When compared to each other, the fluorescence intensity maximum, in the contour peak 1 corresponding to that of the crude oil sample, was not substantially different from one another, e.g. GILA samples were 4, 4, $7x10^5$ CPS/μA, and VBLA samples were 8 and 3 $x10^5$ CPS/μA. It suggests there was not substantial difference in crude oil exposure among the fish caught from VBLA and GILA, although VBLA was not in direct path of the oil spill. This is possibly due to menhaden being migratory fish and they may have ingested contaminated foods (oil droplets, zooplankton, phytoplankton and organic debris) in their migratory path. It is possible that as the spill was dispersed, that the crude oil spread into areas like Vermillion Bay and then accumulated into the fish as they migrated to and from the estuary. All the fish caught for this study were about 1-3 years of age, and should had experienced at least one migration. If

we could compare menhaden young of the year (0-age), and observing 0-age menhaden from VBLA having substantially less crude oil fluorescence in its tissue than that from GILA would give evidence to PAH laden Gulf menhaden migratory path.

Among the five liver samples, three samples (GILA520L, VBLA272L and VBLA270L) showed a second contour center in the EEMS (lower left, Fig. 5G, I, J). We could disregard this contour peak as contamination of albumin or other fluorescent biomolecules in the liver samples. However, it was interesting to notice that these three EEMS shared one feature: the emission wavelength of the first contour center were 10 – 15 nm longer (red-shift, to 440 or 445 nm) than that of crude oil which was at 430 nm; in contrast, the contour center emission wavelength for the other two liver samples that did not have a second center (GILA420L and GILA531L) were 435 nm, only 5 nm longer than that of the crude oil sample. (Fig. 5D, H). It suggests that degradation of LMW PAHs in these three samples were to a greater extent, thus shifting the PAH composition even more toward HMW which fluoresce at longer emission wavelength.

In agreement with this, the specific position of 2nd contour peak (approximately 290/340, 285/320, 275/330 nm, ex./em., for GILA520L, VBLA272L and VBLA270L respectively) suggests that these liver samples contained PAH metabolites of very low aromaticity. They could be as low as 1-aromatic ring conjugated with zero or one or two additional unsaturation. Earlier work with PAH standards showed that vitamin E, a compound with 1-aromatic ring conjugated with 1 non-aromatic ring, fluoresced with a contour center at 290/330 nm, while 2-naphthol

, among the smallest LWM PAHs, had EEMS contour center at much longer emission wavelength already (285/355nm, ex./em., Pena et al., 2015). Thus the specific position of this 2nd contour peak, if not fully accounted for by albumin or biologically native counterparts, indicating

that in-depth PAH degradation may be producing metabolites of very low aromaticity (i.e. possibly only one or no aromatic rings as compared to its parent structure).

In summary of the liver sample EEMS comparison, the red-shift of crude oil PAH couture center suggests LMW PAHs were being degraded in menhaden liver tissues, and this was observed in all five liver samples analyzed. The extent of red-shift was greater in three of the five liver samples, which was accompanied by the appearance of a second contour center, both supporting in-depth metabolism of LWM PAHs as to produce metabolites of low aromaticity.

This result from 3D EEMS was also backed by the 2D fluorescence scans (Figure 6). Liver, followed by Gonad and Gill had the largest crude oil signature (i.e. excitation wavelength 360nm and emission 440nm). Interestingly enough, crude oil signatures present in different organs support the conclusion that polymorphisms from these organs are then possible. In conclusion of PAH fluorescence analyses should expand EEMS data onto larger groups of Gulf Menhaden to further verify crude oil profiles trends are consistent in other fish.

Figure 5. 3D Excitation Emission Spectroscopy

Figure 5: For these 3D EEMS scans, relative PAH presence was determined by the florescence intensity in high excitation & emission wavelength areas, where the higher the excitation and emission wavelength are, more aromatic rings the compound is associated with. Standards were used as controls and aside from crude oil, the other biologically derived standards (i.e. NADH, nucleotides, Vitamin A, Vitamin E, and Albumin) did not represent biologically relevant quantities (i.e. x500 as much was used to get an observable signal). All sample scans had a blank 75% ethanol solution fluorescence scan subtracted to provide the displayed fluorescence scans. In Figure 5A-C, the proper solvent concentration was determined by which as much of the excitation and emission signals could be detected and differentiated from other biologically relevant compounds (e.g. albumin, Vitamin A, Vitamin E; Vitamin A and Albumin areas are circled). The best solvent was determined to be 75% ethanol because it met these criteria. In regard to interpreting the fluorescence, in Figure 5A-F, dark gold is considered low fluorescence whereas bright red represents a high fluorescence signature. Figure 5G-J is true in the opposite case, as in, bright red represents low fluorescence intensity and dark gold represents high fluorescence intensity. In Figure 5D-J, GILA 420L, D, & G were run in 75% ethanol and tested to confirm if crude oil was present in the tissue. Interestingly, only GILA 420 (Figure 5D-F) and 531L (Figure 5H) samples do not show PAH derived crude oil metabolism, whereas Figure 5G, I and J did. PAH metabolism is visualized by the EEMS scan as a fluorescent smearing which takes the pure crude oil signature (Figure 5A-C) and spreads the fluorescence to the bottom right hand portion of the graph. Contour peaks 1 (Figure 5A-J) and 2 (Figure 5G, I, and J) were identified as well and stared as compared to Figure 5B.

Figure 6. 2D Excitation Florescence Spectroscopy

Figure 6: These 2D Excitation Florescence graphs work in with in the same way as the 3D EEMS; at one only emission wavelength (i.e. 440nm emission), a spectra of excitation lengths were recorded from several GILA samples. 440nm emission was selected specifically because it overlaps where the strongest crude oil florescence signature is; in addition to having the strongest peak at an excitation wavelength of 360nm. All sample scans had a blank 75% ethanol solution fluorescence scan subtracted to provide the displayed fluorescence scans. Like in the 3D EEMS scans (Figure 5), the organ that has the most florescence is liver, but noticeable peaks are also present in the gill and gonad.

Gulf Menhaden physical features - Log Mass vs Log Length

These length and mass measurements were taken prior to dissection in order to determine the approximate ages of each school of fish from one another, where all fish were dated at the time of collection and placed on a logarithmic graph.

Overall, fish demonstrate a similar correlation to Jr., et al.'s (2016) and Turner's data (2017). Late Summer and Summer GILA fish are about 0-1 years while 2012 GILA fish range from 1 year old (n=4) to 2 years old (i.e. Summer VBLA) (Figure 7C) (Jr, et al. 2016). Interestingly, VBLA fish are far more variable than GILA during the same time frame, which was an unexpected result (Figure 7A). VBLA could not be dated reliably from turner's data, as the fish did not have clearly linear trends, but are at least 2 years old (Figure 7C).

The trend exhibited by the summer and late summer GILA does not assume a linear relation like the rest of the data, but rather a parabolic shape, suggesting some developmental irregularities are occurring as well. This result may be due to endocrine disruption from the crude oil derived PAHs' estrogenic qualities inducing abnormal spawning patterns, which is seen in Jr., et al's study as well during 2013 (2016). The hurricane that passed through the area in 2012 may have also redistributed the crude oil trapped in the sediment (Olson, et al. 2016). The 2012 Fall GILA fish also appears to be fairly parabolic as well, but that unfortunately could be determined due to the small number of fish samples. Age differences in the fish are not expected to be significant issue as most fish only live up to 1 to 2 years of age and with an average life span of 5-6 years (Louisiana 2018; Turner 2017).

As far as the Menhaden schools are concerned, there seems to be two schools present during the same year and season for GILA fish (Figure 3C). Represented by to distinct, parallel lines, both Summer and Late Summer GILA fish. The top group of 2013 Summer and Late Summer has a higher log length per log mass than the bottom group. The differences between

these groups is most likely due to two different schools of GILA that were caught at the same time. In this case, it is not expected that there were any significant differences because of this different school as both schools do not deviate from the expected growth trend. (Jr. et al. 2016; Turner, et al. 2017). Futures studies will aim to expand current data onto large fish collections and assess the statistical significance of these trends.

Figure 7. Log Mass vs Log Length in VBLA and Gila Fish Comparison

Figure 7: These length and mass measurements were taken prior to dissection in order to determine the approximate ages of each school of fish from one another. All fish were dated at the time of collection and placed on a logarithmic graph. Overall, fish demonstrate a fairly strong correlation (i.e. $R^2 = 0.8816$) and according to Turner's (2017) and Jr, et al. data (2016), all VBLA and GILA fish are about 2-3 and 1 years old respectively, with exception to samples GILA 562, 564 (both spawned during the same year) and 2012 GILA fish (approximately 2 years old) (Jr, et al. 2016). Interestingly, Fall GILA 2013 and 2012 fish are parabolic in shape and does not assume a linear relation like the rest of the data. VBLA fish are extremely variable and do not assume any linear trends predicted by Jr, et al. (2016) or Turner's (2017) data. Aside from this findings, age differences in the Gulf Menhaden fish are not expected to be significant due to most fish only living up to 1 to 2 years in the wild, even though they may live up to 5-6 years if not prematurely killed (Jr, et al. 2016; Turner 2017).

DNA Sequencing Results and Amino Acid Equivalents

While SSCP was useful to discern the occurrence of major insertion and deletion mutations in *p53* DNA binding region in menhaden, DNA sequencing allows us to resolve nucleotide substitution mutations as well. The substitution mutations would cause change in amino acid sequence, i.e. missense mutations was of particular interest as it may disrupt the P53 functioning.

In order to analyze how *p53* DNA biding region polymorphisms were manifested in amino acid sequence, the PCR products from VBLA276H (SSCP at Lane 6 Fig. 4D) and GILA527L (SSCP at Lane 4 Fig. 4C) were cloned, and one clone from each were sequenced. Two sequences of 348 and 363 bp were resulted for VBLA276H and GILA527L respectively. The nucleotide sequences (with introns) were converted into amino acids sequences (with 2 nt shift downstream for reading frame) and were compared against that of *Fundulus heteroclitus* (Atlantic Killifish) cellular tumor antigen *p53* isoform X2 (without intron) and against each other (Figure 8).

Both sequences lined up well with that of killifish's and were nearly identical in the exons (Figure 8A, B, red boxed areas). The only difference was that a cysteine (amino acid 211, C, in the first exon of the killifish sequence) was changed into serine (S) in VBLA 276H, and a leucine (amino acid 237, L, in the 2nd exon the killifish sequence) was changed into a serine (S) in GILA 527L. A major non-identity were found in VBLA 276H and GILA 527L in Figure 8C corresponding to the intron which was not included in the killifish's sequence (Figure 8A blue boxes), but not for the GILA 527L sample. When the menhaden sequences were aligned against each other, VBLA 276H and GILA 527L were 79% (103/131) identical and 80% (105/131) positive. Three types of differences were observed. a) The two amino acids in exons mentioned earlier, from S (serine) in VBLA to C (cysteine) in GILA in the 1st exon and L (leucine) in

GILA to S (serine) in VBLA in the 2nd exon. This would directly affect the amino acid sequence in P53 DNA Binding Domain. b) 5-amino acid long gap in the intron, VBLA276H intron area was 15 bp shorter than GILA527L (Figure 8). c) Replacement in the intron area: two positive replacement (I → M, K →Q; all showing VBLA276H → GILA527L), and eight non-positive replacement (D→V, L→F, L→S, K→N, N→Q, V→P, I→H, L→P) (Figure 8C. Although the latter two differences affected the introns only, at times the mutated intron can become important, for example, inducing intron retention mutation, which would then result in major changes to the protein that the sequence codes for, for example, additional splice sites which would lead to protein truncation (Piasecka, et al. 2015).

Now with the menhaden *p53* DNA binding region sequence available, further analysis was done to analyze the single stranded nucleotide structure (Fig. 9). It turned out that, when single stranded, the 1st exon, 1st exon+intron, the 2nd exon, and the 2nd exon+intron may assume elaborate hairpin structures with the calculated melting temperatures possibly relevant to the PCR program (Fig. 9 A – H, elaborate hairpins circled), and it was the same for killifish exons (Fig. 9 I – K). This suggests that PCR artifacts, especially the 1st, 2nd exon with melting temperature at ~ 50 ^{o}C, may contribute to the amplification of single stranded DNA of unexpected sizes, which may appear in agarose gel electrophoresis as fuzzy bands of smaller sizes (e.g. Fig. 3B, and C). The initial cloning and sequencing work (which was done to confirm the custom designed PCR primers amplified *p53* DNA binding region in menhaden) did reveal a truncated DNA sequence from GILA527L that contained the 1st exon only (Fig. 9L). It was possible that during this primer set F4/R1 testing PCR only the F4 primer was working and that after leaving the first exon, Taq polymerase was unable to complete the rest of the sequence, thus a truncated PCR product. However, when the proper primer set (F4/R0) were used, hairpins

induced PCR artifacts should be insignificant among the PCR products, as F4/R0 consistently generate sharp single band of ~ 360 bp in agarose gel electrophoresis for most samples (e.g. Fig. 3A), thus their contribution to SSCP polymorphism pattern should be insignificant. Thus our preliminary results suggest that the polymorphisms observed in SSCP were unlikely of PCR artifacts but real to the menhaden samples, and that low rate of missense mutations were occurring in the 1st and 2nd exons in addition to multiple nucleotide substitution and stretch of nucleotide insertions in the intron. Additional cloning and sequencing data could be used to strengthen the conclusion.

Figure 8. VBLA and Gila Clone Amino Acid Equivalent Comparison

VBLA 276H vs Atlantic Killifish Amino Acid Sequence Match

GILA 527L vs Atlantic Killifish Amino Acid Sequence Match

VBLA 276H vs GILA 527L Amino Acid Sequence Match

Figure 8: Figure 8A, B, and C were all nucleotide sequence data was converted into relevant amino acids as to confirm how the actual exons line up with one another as to elucidate how polymorphisms changed into a peptide sequence. Overall identity for VBLA and GILA were 51% and 89.3% respectively to the Killifish. If the nonshared intron sequence is removed from VBLA, the identity between VBLA to Atlantic Killifish would be 90.8%. The Atlantic Killifish mRNA considered does not have an intron, but the match (i.e. blue box in Figure 8A) has recognition with the beginning part of the second *p53* exon. Only the end portion of the GILA sample's intron is recognized when compared to the Atlantic Killifish mRNA (Figure 8B Blue Box). VBLA possesses a cysteine to serine mutation in the 1st exon (Figure 8A), but GILA lacks this mutation (Figure 8B). In addition, GILA has a leucine to serine mutation in the 2nd exon (Figure 8B), when compared to the killifish p53 sequence, while VBLA lacks this mutation (Figure 8A). If both the VBLA and GILA sequences were directly compared to one another, GILA, along with having 5 amino acids each, has lysine to asparagine/glutamic acid, leucine to phenylalanine, asparagine to glutamic acid, leucine to serine, aspartic acid to stop codon, valine to tyrosine, and leucine to proline mutations in the intron region.

Figure 9. GILA, VBLA and Killifish Hairpin Analysis

VBLA 276H P53 1st Exon Hairpin with F4 Tm: 53.5°C

VBLA 276H P53 1st Exon Hairpin & Intron with F4 Tm: 40.4°C

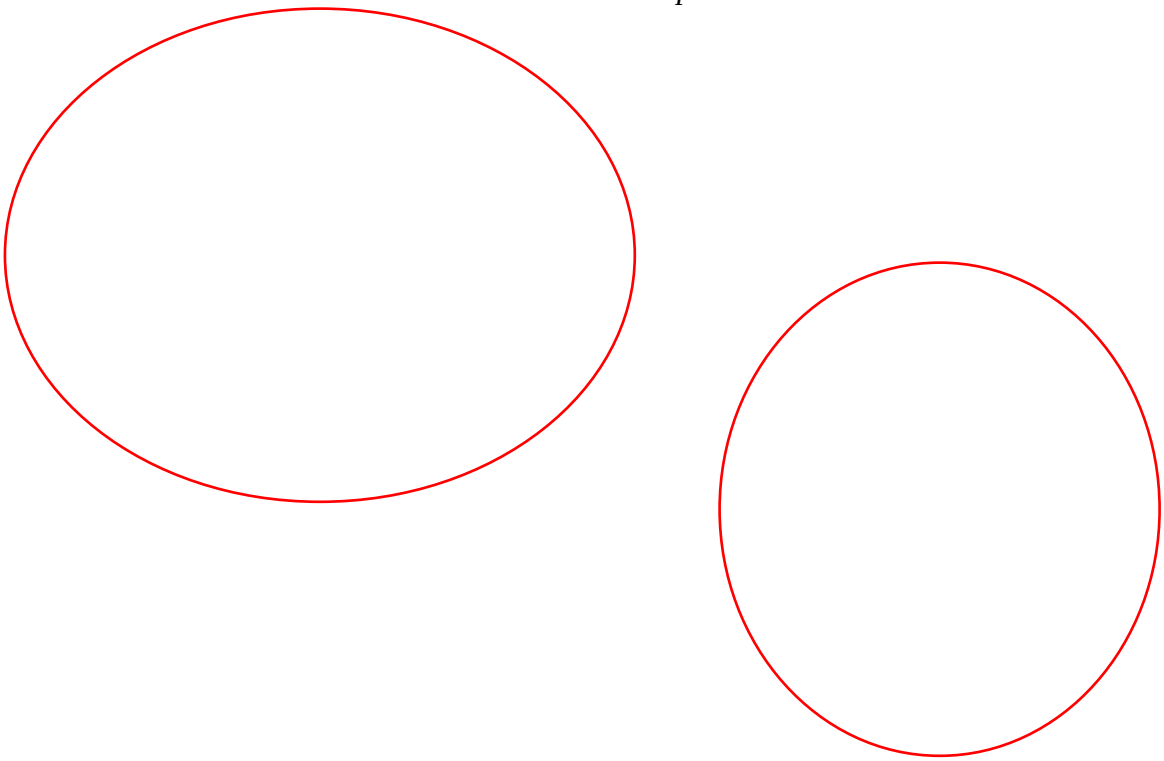

VBLA 276H P53 2st Exon Hairpin with R0 Tm: 48.2°C

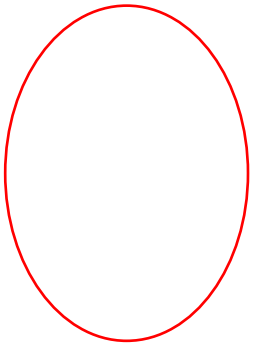

VBLA 276H P53 2st Exon Hairpin & Intron with R0 Tm: 38.4°C

GILA 527L P53 1st Exon Hairpin F4 Tm: 51°C

GILA 527L P53 2nd Exon Hairpin Tm: 46.8°C

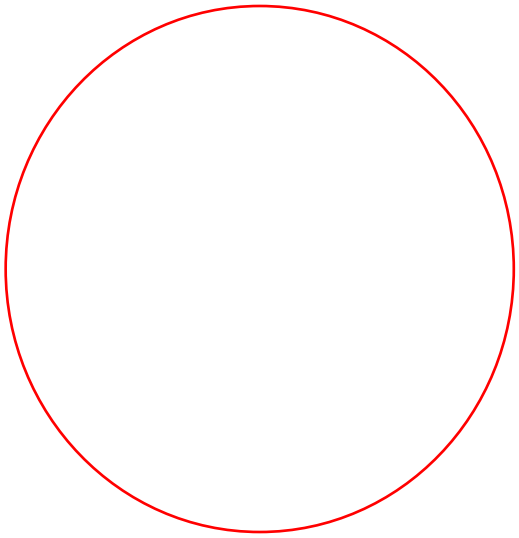

GILA 527L P53 1st Exon Hairpin & Intron with F4 Tm: 42.4°C

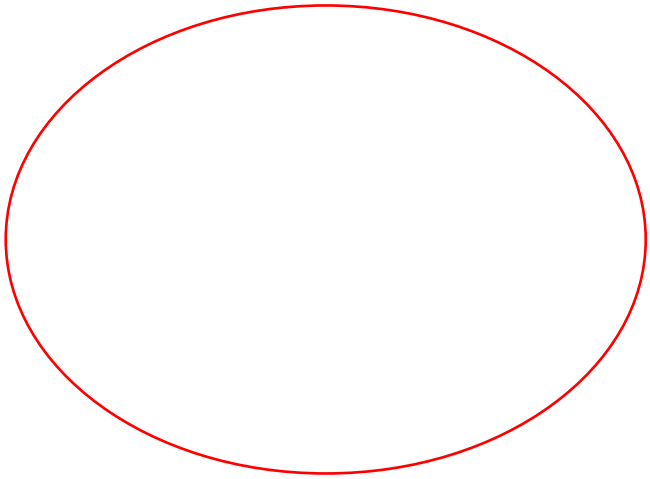

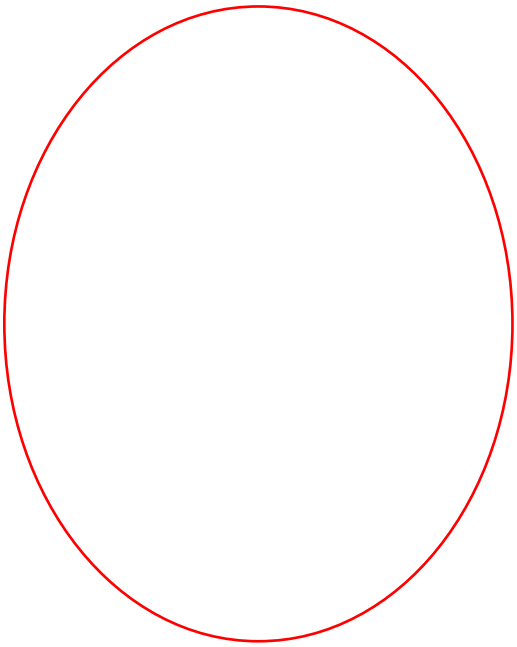

GILA 527L P53 2nd Exon Hairpin Tm: 46.8°C

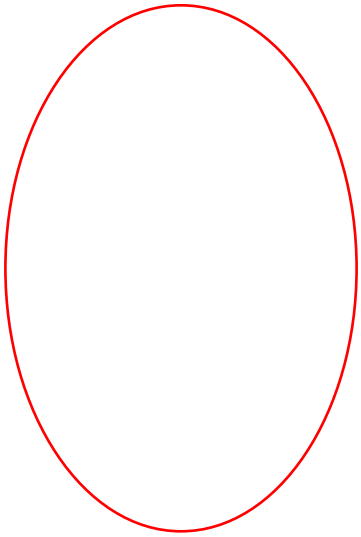

GILA 527L P53 2nd Exon Hairpin & Intron with F4 Tm: 45.9°C

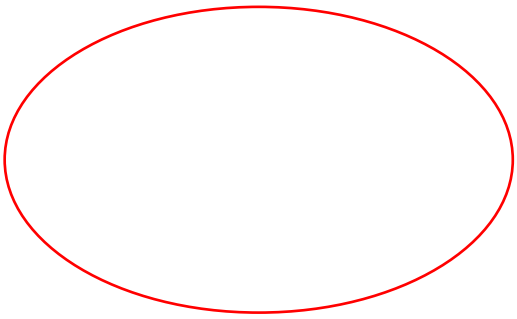

Atlantic Killifish DNA Equivalent of 1st and 2nd Exon Tm: 48.3°C

Atlantic Killifish DNA Equivalent of 2nd Exon Tm: 48.2°C

Atlantic Killifish DNA Equivalent of 1st Exon Tm: 48.4°C

Truncated GILA 527L Hairpin Structure Tm: 46.6°C

Figure 9: Figure 9A-L were single stranded DNA hairpins found via using Genescript's DNA Sequencing service for samples VBLA 276H and GILA 527L with the primer set F4/R0. *P53* DNA Binding Region had to be split between the 1st exon-intron and intron-2nd exon portions in order to be read. The primer labeled with each segment is to inform the reader where in the DNA Binding Region that hairpin structure is located. Hairpin dissociation temperatures were included as a crude measure of thermo-stability and does not account for salt and dNTPs present in actual conditions. Hairpin structures of particular interest are circled. In Figure 9I, J and K, Atlantic Killifish DNA equivalents resembled VBLA 1st and 2nd exons, which may suggest that VBLA have less harmful polymorphisms than GILA does. Figure 9L, is the 1st exon hairpin at the original truncated GILA 527L sample. The hairpins present in this structure is believed to have collapsed the Taq polymerase's replication fork after the first exon and, as a result, made it unable to synthesize the whole *P53* template sequence.

Discussion

It was hypothesized that a functional *p53* primer set can be derived for Gulf Menhaden from the previous work on Atlantic Killifish sequence to amplify menhaden's *p53* DNA binding region. This is because *p53* DNA binding region is typically conservative across species.

Overall, the *p53* primer set developed from Atlantic Killifish sequencing data (Nadler, et al., 2017) did work. It was expected that primer sets with the highest Gibbs free energy (delta G) value for homo/heterodimerization would provide the sharpest bands. This eliminates the use of primers F4 and R3, and the pairing of F3/R0 (Figure 2E). Both primer sets F3/R2 and F3/R1 fit this description; however they did not produce a single band at about 360bp [Figure 3B and C] but produced a profile with a main band at 150 and 50bp respectively, which could be due to the reverse primers exhibited stronger than predicted self dimerization (Lepre, et al. 2017; Uversky 2016). The strong 150bp during primer testing (figure 3B) is most likely due to the high annealing temperature being high enough for the Taq polymerase to synthesize the first exon using the F4 primer, but not enough to prevent hairpin structure formation, which may cause the replication fork to collapse and forced the polymerase to dissociate (Figure 2H; Yeo, et al. 2016).

Single stranded DNA hairpin interference is supported by the fact that the 1st exon and intron have an elaborate predicted single stranded DNA hairpin structure and a high predicted dissociation temperature (Figure 2G, H, I, and J). This conclusion is consistent with other literature where this same phenomenon is observed in *in vitro* cell cultures and is suspected in cancer patients (Brázda, et al. 2017; Yang, et al. 2012; Yeo, et al. 2016). However, F4/ R0 provided a consistent and strong band for each menhaden sample that tested (Fig. 3b), which was not expected. The discrepancy may be due to different salt and dNTP concentrations in PCR reaction that were not accounted in the prediction using in the Gibbs free energy values.

It was intended that any insertion/deletion polymorphisms could be detected in the PCR-SSCP. One band at about 360nt was expected for GILA as the normal profile, whereas insertion or deletion mutations would result in a profile with different band(s) size. PCR-SSCP was reported to sensitively detect single nucleotide insertions/deletions for smaller sequences (i.e. less than 200nt) (Hayashi, et al. 1992; Sunnucks, et al. 2000). The sensitivity reduces for larger sequence. For our samples, we were able to distinguish between a 20nt difference in a 360nt template (Fig 3B; 4). This is to say that the approximate difference in intron size between VBLA and GILA samples.

Pattern II, with bands at 360 and 200 nt, were typically present in SSCP gels of the samples, but only Pattern I, with a band at 360 nt, was observable in the agarose gels (Figure 4H). The only major differences between the SSCP and agarose gels was the dye used to stain the DNA, and that SSCP separates and denatures DNA into linear single strands. Of these two points, the DNA stain is the most likely to produce a difference. Since Ethidium Bromide and SyberGold were used in the agarose and SSCP gels respectively, 1x SyberGold dye is 100 to 25 times more sensitive than Ethidium Bromide in detecting DNA according to Thermofisher product information (Syber 2018). Being that the same samples that were run through SSCP also were run through agarose gels, it is most likely that the second band is below detectable concentration of the Ethidium Bromide, only visible when running SyberGold. The notable exceptions to the 2-band SSCP patterns were GILA 562L and GILA 521M, VBLA 279M, VBLA 276M and VBLA GILA 556H (Figure 4B, C, and G). In particular, GILA 562L, the smallest fish of among all the samples, is speculate that this deviation is possibly due to this fish being spawned from a parent that developed during the BP oil spill (Jr., et al. 2016) given the

approximate size and weight of this fish in addition to fecundity of Gulf Menhaden spiking up two to four years post Deepwater horizon oil spill (i.e. higher than prior years).

The 200bp band size coincides with *p53* DNA binding domain after the intron removal or one of the exons (i.e. 1st or 2nd exon) with the intron attached (Figure 9A-H). The former reason is consistent with dogma in the sense that the introns are spliced out in order to yield a function protein, which may be occurring as the major *P53* profile. The latter reason is also plausible due to possible alternative splicing (Yeo, et al. 2016) or hairpin formation of the DNA strand (Figure 9A-H). Alternative splicing is reported to be very common with *P53*, where portions of the intron may also be included in the functional protein (Lepre, et al. 2017; Uversky 2016; Yang, et al. 2012). In regard to hairpin formation, if certain key mutations are present in the nucleotide sequence, it may cause the associated enzymes to become unable to recognize the DNA binding domain (i.e. failing to associate to the sequence) as well as cause transcription factors to become unable provide adequate support during transcription (Brázda, et al. 2017; Lepre, et al. 2017; Uversky 2016; Yeo, et al. 2016). Mutation-instigated stabilization of single stranded DNA secondary structures may cause double stranded breaks, collapse the replication fork, and further form abnormal DNA recombinants and deletions (Yeo, et al. 2016). In this context, it is not surprising that P53 preferentially binds to DNA secondary structures, supercoiled DNA, and DNA mismatches which strengthen P53 repair signaling function demonstrated in previous literature *in vitro* and *in vivo* (Brázda, et al. 2017; Lepre, et al. 2017; Uversky 2016; Yeo, et al. 2016). This preference could also promote other functions of P53 aside from repair, but this aspect is still being studied.

In context of the hairpin perspective, is also backed by Figure 9A-H found in this study, where GILA exhibited secondary structures that may inhibit P53 over VBLA (Figure 9A-H

(Brázda, et al. 2017; Lepre, et al. 2017; Uversky 2016; Yeo, et al. 2016). GILA lacks hairpin complexity in the second exon (Figure 9G and H), but does not resemble normal Atlantic Killifish *p53* DBR hairpin formation (9J and K). GILA also has a lower dissociating temperature than the VBLA sequence or Atlantic Killifish *p53* 2nd exon hairpin equivalent (Figure 9C, D, H, H, J and J). These findings support a possible reduction P53 recruitment to the DNA Binding region domain and inhibition of *p53* expression in GILA. This is important because if transcription was terminated midway into the *p53* DNA Binding Region (Figure 1), then truncated, nonfunctional P53 would be produced (Brázda, et al. 2017; Lepre, et al. 2017; Uversky 2016; Yeo, et al. 2016). VBLA hairpins (Figure 9C and D), on the other hand, more closely resemble their conserved Atlantic Killifish equivalents (Figure 9J and K). Specifically, both the 1st and 2nd exons in both fish (Figure 9C, D, J and K) are more similar than VBLA to GILA (Figure 9G and H) for both exons. Hairpins in the intron also appear to be off by one between samples, which may be involved with alternative splicing and/or intron retention. Overall, abnormal hairpins formation were present, but further analysis would be required to determine how these specific hairpin formations interact with *P53* function.

It may be assumed that these individuals were less affected by the crude oil than the others. There are a number of ways that this could be but it is most likely be that these fish developed other mechanisms to better deal with the crude oil than the rest of their school. This finding best represents the bottleneck effect, which restricts an original population to only those individuals who can better cope with particular stressors. Menhaden fish may achieve this either through more active P53 or PAH metabolism (Bentivegna, et al 2016; Millemann. et al. 2015); however, both options may not successfully counteract the crude oil/crude oil derived PAHs' effects on endocrine disruption. If endocrine disruption is involved, it may explain the

discrepancy between the SSCP band patterns and the development trend data (Figure 4; 7). Further expansion of current study with additional fish and cloning/sequencing would further confirm and elucidate these results.

It is possible that the crude oil exposure was more disruptive to the younger fish, especially when they go through substantial growth and development. Crude oil and crude oil derived PAHs may interfere with development by preventing P53 from properly functioning in embryotic development as well as disrupt the endocrine system by being an estrogen mimic. (Antoun, et al. 2018; Barthelery, et al. 2016; Bugel, et al. 2014 Lepre, et al. 2017; Uversky 2016; Van Drooge, et al. 2017; Zadlock 2017). If a fish survives P53 damage prior to birth or during early development will likely not assume normal length and weight trends due to *P53* inhibition, but there is a confounding effect of PAHs, where if they interact with estrogen receptors, may also cause a similar outcome as crude oil derived PAHs may have on P53 function. If the menhaden fish downregulate their estrogen receptors like what is found in Bugel et al.'s Atlantic Killifish, they may be as not affected by the crude oil (Antoun, et al. 2018; Barthelery, et al. 2016; Bugel, et al. 2014; Turner 2017; Van Drooge, et al. 2017; Zadlock 2017). This adaptation does cause issues during embryotic development, but would protect the menhaden fish from otherwise potentially acute disruption, as the PAHs present in the water column exceed estrogen's biologically relevant blood plasma concentration (Antoun, et al. 2018; Barthelery, et al. 2016; Bugel, et al. 2014 Lepre, et al. 2017; Uversky 2016;Van Drooge, et al. 2017; Zadlock 2017).

This endocrine disruption trend was supported by Figure 7, but was opposite to the original hypothesis. Irregular parabolic weight to length pattern by the 2012 Fall GILA fish (Figure 7A and C) and development in VBLA fish was found more variable than other expected

data (Louisiana 2018; Turner 2017). Being that these GILA fish were caught in September, this finding would correspond to the beginning of the spawning season for Gulf Menhaden and support persistent crude oil interference during embryological development. But in terms of overall development, VBLA was more variable than GILA fish and did not have consistent linear trends (Figure 7). These results were consistent with the overall finding that 2012 and especially 2013 that the fecundity of Gulf Menhaden did spike up two to four years post Deepwater horizon oil spill (Jr., et al. 2016).

As for the EEMS and 2D scans (Figures 5 & 6), all samples exhibited the same signal pattern as pure crude oil, with GILA samples GILA 420 L, D, G and GILA 531L displaying little PAH metabolite presence. PAH metabolites would appear as a fluorescent smearing of the sharp crude oil pattern exhibited in Figure 5A, B, and C as shown in Figure 5G, I, and J. This findings suggests that some samples degrade PAHs but there appears to be hindrance in the case for certain GILA samples. This conclusion makes sense considering that EEMS and Fluorolog can detect PAHs in the nanogram range, and that in attempt to prevent further DNA damage, active PAH metabolism would be present. The SpectraMax can only visualize one emission wavelength (Figure 6) regarding PAH degradation, but it definitely shows PAH presence in various tissues in a short period of time (Figure 6). As far as the organs compare, the strongest crude oil intensity was in the liver samples of 2012 GILA Fall fish, followed by gonad and gill (Figure 6). Interestingly, although the gill tissue had the weakest intensity compared to other organs, the SSCP gels for samples still exhibited the second 200bp band supporting our hypothesis that although not as fatty as other organs, the DNA repair mechanisms for Menhaden Gills may not be sufficient to handle PAH induced polymorphisms hence why the second band variant is there. Further cloning and sequencing of this second band would be required to confirm this

conclusion.

In regard to the clones, the cloned P53 sequences best resembled Atlantic Killifish in NCBI BLAST search because not much information regarding Gulf Menhaden's transcriptome is present (Figure 8). Aside from this, there were particular polymorphisms that occurred in that seemed to strengthen P53 function for GILA fish (Figure 8). GILA Mutations as compared to VBLA included in the first exon a serine to cysteine shift whereas the second exon had a leucine to phenylalanine/proline/ serine shift (Figure 8C). This is important because the phenylalanine, proline, and serine amino acids all impact these introns in different ways (Jung, et al. 2015; Lao, et al. 2017; Schlereth, et al. 2013; Retzlaff, et al. 2013; Roth, et al 2000). Phenylalanine helps stabilize P53 subunits to target DNA sequence, while serine increases nuclear localization of P53, tetramerization, and transcription (Jung, et al. 2015; Lao, et al. 2017; Schlereth, et al. 2013; Retzlaff, et al. 2013; Roth, et al 2000). This could aid GILA fish to be more resistant to PAHs by inducing damaged cells to repair damaged DNA and induce apoptosis if the DNA is unable to be fixed (Figure 8B and C). The biggest issue would be with the second function of Phenylalanine in the first exon and proline in the second exon for GILA (Figure 8B and C). Proline severely disrupts DNA binding region as it converts the protein into a trans configuration and forces the protein to be unable to bind to the DNA sequence (Jung, et al. 2015; Lao, et al. 2017; Schlereth, et al. 2013; Retzlaff, et al. 2013; Roth, et al 2000). Phenylalanine, on the other hand, can disrupts the tetramerization of the P53 protein post-translation and may not allow it to properly read DNA sequences or associate to proteins (Lepre, et al. 2017; Schlereth, et al. 2013; Uversky 2016). This strange combination suggests that *P53* has an optimization threshold where, under stress, may induce select mutations in order to induce P53 function, but once past that threshold, becomes unable to cope with xenobiotic insults. At this state, P53 may become nonfunctional, or even

antagonize with an otherwise normally functioning P53 tetramer, resulting in inhibition *P53* function. (Joerger, et al. 2014; Jung, et al. 2015; Ho, et al. 2015; Lao, et al. 2017; Schlereth, et al. 2013; Retzlaff, et al. 2013; Roth, et al 2000). Future work seeks to obtain additional sequencing data to validate these trends in Gulf Menhaden fish as well as to determine how exact DNA Binding Region polymorphisms affect P53 function.

As for VBLA fish (Figure 8A), all of the polymorphisms occurred in leucine amino acids which contribute to P53 stability but not a significantly as phenylalanine, serine and proline do (Joerger, et al. 2014). This finding is similar to Mordukhovich, et al.'s study, where they found that P53 mutations associated with PAHs in P53 active cancers were inversely related; however, P53 Mutations were positively related in those with P53 inactive cancers (2010). In that case, since high affinity P53 DNA binding domains are associated to more pro-arrest, than low affinity domains, which promotes more cell death (Lepre, et al. 2017; Schlereth, et al. 2013; Uversky 2016), this would further support that both VBLA and GILA fish were impacted by crude oil and crude oil derived PAHs, which is an unexpected result (Schlereth, et al. 2013). Most studies did not account for PAH concentrations past 2011. Upon further study, with exception to one study, literature backs that GILA was indeed more contaminated than VBLA initially, but toward 2012, increased in pollution validated via Synthetic-aperture radar satellite imaging and PAH sampling via sediment core (Adhikari, et al. 2016; Daly, et al. 2016; Oslon, et al. 2016; singleton, et al 2016). In Oslon's study, both PAH analyses of sediment cores and Menhaden fish VBLA and GILA locations were not significantly different, but is significantly different from 2011 and 2013 (2016). A slight, nonsignificant increase was also present in menhaden fish during 2013, which is not believed to represent a new PAH source, but rather the stirring of contaminated sediment that reintroduced Menhaden fish to PAH containing crude oil, which is most likely due to the

hurricane that passed through the region during that time (Adhikari, et al. 2016; Daly, et al. 2016; Oslon, et al. 2016; singleton, et al 2016). This study's findings also support this conclusion.

Conclusion

Overall, preliminary results find that both VBLA and GILA fish were impacted by crude oil and crude oil derived PAHs from the Deepwater Horizon Oil spill. Differences between VBLA and GILA are most likely due to the Bottleneck effect, which may be induced at a molecular level by crude oil, which as the original population is exposed to a stressor, only the select few in that species survive. Others that cannot die off, like in the case of VBLA fish due to their overall development trends compared to GILA, polymorphism patterns, and DNA secondary structure (Figure 2G-M, 4, 7, 8). In Figure 4, overall a similar profile, two band P53 profile was observed, with a few exceptions from GILA suggesting maladaptive polymorphisms in the DNA Binding region. Fluorescent scans indicate that certain organs did retain more PAHs than others, but more samples would need to be examined to determine overall consistency of fluorescence profiles over more VBLA and GILA fish (Figure 5, 6). PAHs from Deepwater Horizon Crude Oil were determined to be associated with direct polymorphisms and dysfunction in P53 once optimization threshold for this tumor suppressor gene has been exceeded. In addition, PAHs were found to be associated with development irregularities in Gulf Menhaden (Figure 7), but further research would be require to verify if this due to P53 interference or via Estrogen mimicry. Futures studies would have to expand current results onto a larger sample size and check for consistency in expanded trends in addition to examining how effects of DNA/ RNA secondary structure on P53 on transcription and translation, determine how polymorphisms resulting in amino acid changes influence P53 binding and function, and observing how expanded Fluorescence, Weigh vs Height, and SSCP profiles correspond to crude oil and crude oil derived PAHs.

Works Sited:

Adhikari, P. L., Maiti, K., Overton, E. B., Rosenheim, B. E., & Marx, B. D. (2016). Distributions and accumulation rates of polycyclic aromatic hydrocarbons in the northern Gulf of Mexico sediments. *Environmental Pollution*, *212*, 413–423.

Anderson, J. D., & Karel, W. J. (2014). Limited genetic structure of Gulf Menhaden (Brevoortia patronus), as revealed by microsatellite markers developed for the genus Brevoortia (Clupeidae). Fishery Bulletin, 112(1), 71–81.

Antoun, S., Atallah, D., Tahtouh, R., Alaaeddine, N., Moubarak, M., Khaddage, A., … Hilal, G. (2018). Different TP53 mutants in p53 overexpressed epithelial ovarian carcinoma can be associated both with altered and unaltered glycolytic and apoptotic profiles. Cancer Cell International, 18, 1–10. https://doi.org/10.1186/s12935-018-0514-2

ATSDR - Case Studies in Environmental Medicine. (2009). Retrieved February 10, 2018. PDF.

Barthelery, N. J., & Manfredi, J. J. (2016). Feature Review: Cerebellum Development and Tumorigenesis: A p53-Centric Perspective. Trends in Molecular Medicine, 22, 404–413.

Brázda, V., & Coufal, J. (2017). Recognition of Local DNA Structures by p53 Protein. International Journal of Molecular Sciences, 18(2), 1–18.

Bentivegna, C. S., DeFelice, C. R., & Murphy, W. R. (2016). Excitation–emission matrix scan analysis of raw fish oil from coastal New Jersey menhaden collected before and after Hurricane Sandy. *Marine Pollution Bulletin*, *107*, 442–452.

Bugel, S. M., Bonventre, J. A., White, L. A., Tanguay, R. L., & Cooper, K. R. (2014). Chronic exposure of killifish to a highly polluted environment desensitizes estrogen-responsive reproductive and biomarker genes. Aquatic Toxicology, 152, 222–231.

Chan, W. M. (2006). Ubiquitination of p53 at Multiple Sites in the DNA-Binding Domain. Molecular Cancer Research, 4(1), 15–25. https://doi.org/10.1158/1541-7786.MCR-05-0097

Chemical and toxicological characterization of sediments along a Colombian shoreline impacted by coal export terminals - ScienceDirect. (2015). Retrieved February 2, 2018.

Daly, K. L., Passow, U., Chanton, J., & Hollander, D. (2016). Assessing the impacts of oil-associated marine snow formation and sedimentation during and after the Deepwater Horizon oil spill. Anthropocene, 13, 18–33. https://doi.org/10.1016/j.ancene.2016.01.006

Diercks, A.-R., Highsmith, R. C., Asper, V. L., Joung, D., Zhou, Z., Guo, L., … Lohrenz, S. E. (2010). Characterization of subsurface polycyclic aromatic hydrocarbons at the Deepwater Horizon site. *Geophysical Research Letters; Washington*, *37*(2).

Genetics; Investigators at California Institute of Technology Report New Data on Genetics (Oxidation of p53 through DNA charge transport involves a network of disulfides within the DNA-binding domain). (2016, February 27). Obesity, Fitness & Wellness Week; Atlanta, p. 896.

Goto, D., & Wallace, W. G. (2011). Altered feeding habits and strategies of a benthic forage fish (Fundulus heteroclitus) in chronically polluted tidal salt marshes. *Marine Environmental Research*, *72*(1), 75–88.

Grazia Marina eQuero, et al. (2015). Patterns of benthic bacterial diversity in coastal areas contaminated by heavy metals, Polycyclic Aromatic Hydrocarbons (PAHs) and Polychlorinated Biphenyls (PCBs). *Frontiers in Microbiology, Vol 6 (2015)*.

Gullett, B. K., Hays, M. D., Tabor, D., & Wal, R. V. (2016). Characterization of the particulate emissions from the BP Deepwater Horizon surface oil burns. *Marine Pollution Bulletin*, *107*(1), 216–223.

Farrington, J. W. (2014). Oil Pollution in the Marine Environment II: Fates and Effects of Oil Spills. *Environment*, *56*(4), 16–31.

Federal Interagency Solutions Group (2010) Oil budget calculator. Report to the National Incident Command, Deepwater Horizon
Hayashi, K. (1992). Review: PCR-SSCP: A method for detection of mutations. Genetic Analysis: Biomolecular Engineering, 9, 73–79.
IUCN. (2012). Fundulus heteroclitus: NatureServe: The IUCN Red List of Threatened Species 2013: e.T189824A18236919 [Data set]. International Union for Conservation of Nature.
IUCN. (2011). Brevoortia patronus: Collette, B., Grubbs, D., Pezold, F., Simons, J., Carlson, J., Caruso, J., McEachran, J.D., Brenner, J., Tornabene, L., Robertson, R. & Chakrabarty, P.: The IUCN Red List of Threatened Species 2015: e.T191208A1972860 [Data set]. International Union for Conservation of Nature.
Joerger, A. C., Wilcken, R., & Andreeva, A. (2014). Tracing the Evolution of the p53 Tetramerization Domain. Structure, 22(9), 1301–1310. https://doi.org/10.1016/j.str.2014.07.010
Johnsen, A. R., & Karlson, U. (2004). Evaluation of bacterial strategies to promote the bioavailability of polycyclic aromatic hydrocarbons. *Applied Microbiology & Biotechnology*, *63*(4), 452–459.
Jmjd5 functions as a regulator of p53 signaling during mouse embryogenesis: Seton Hall University Libraries. (2016). Retrieved April 26, 2018, from
Jr, N. G. G., & Blankenship, C. (2016). Gulf States Marine Fisheries Commission Commissioners and Proxies, 75.
Jung, H., Lee, D., Lee, J., Park, D., Kim, Y. J., Park, W.-Y., … Lee, E. (2015). Intron retention is a widespread mechanism of tumor-suppressor inactivation. Nature Genetics, 47(11), 1242–1248. h
Kadri, T., et al. (2017). Review: Biodegradation of polycyclic aromatic hydrocarbons (PAHs) by fungal enzymes: A review. *Journal of Environmental Sciences*, *51*, 52–74.
Kondo, Y. (2009). Epigenetic Cross-Talk between DNA Methylation and Histone Modifications in Human Cancers. Yonsei Medical Journal, 50(4), 455.
Llamas, A., et al. (2017). Polycyclic Aromatic Hydrocarbons (PAHs) produced in the combustion of fatty acid alkyl esters from different feedstocks: Quantification, statistical analysis and mechanisms of formation. *Science of The Total Environment*, *586*, 446–456.
Lepre, M. G., et al. (2017). Insights into the Effect of the G245S Single Point Mutation on the Structure of p53 and the Binding of the Protein to DNA. *Molecules*, *22*(8), 1–17.
Ley, S. H., et al. (2016). Contribution of the Nurses' Health Studies to Uncovering Risk Factors for Type 2 Diabetes: Diet, Lifestyle, Biomarkers, and Genetics. *American Journal of Public Health*, *106*(9), 1624–1630.
Lindgren, J. F., et al. (2017). Induced tolerance in situ to chronically PAH exposed ammonium oxidizers. *Marine Pollution Bulletin*, *120*(1), 333–339.
Louisiana Fisheries - Gulf Menhaden. (2018). Retrieved April 20, 2018
Liao, P., Zeng, S. X., Zhou, X., Chen, T., Zhou, F., Cao, B., … Lu, H. (2017). Article: Mutant p53 Gains Its Function via c-Myc Activation upon CDK4 Phosphorylation at Serine 249 and Consequent PIN1 Binding. Molecular Cell, 68, 1134-1146.e6.
Mason, O. U., Hazen, T. C., Borglin, S., Chain, P. S. G., Dubinsky, E. A., Fortney, J. L., … Jansson, J. K. (2012). Metagenome, metatranscriptome and single-cell sequencing reveal microbial response to Deepwater Horizon oil spill. *ISME Journal: Multidisciplinary Journal of Microbial Ecology*, *6*(9), 1715–1727.
McCann, M. J., et al. (2017). Key taxa in food web responses to stressors: the Deepwater Horizon oil spill. *Frontiers in Ecology and the Environment*, *15*(3), 142–149.

Millemann, D., Portier, R., Olson, G., Bentivegna, C., & Cooper, K. (2015). Particulate accumulations in the vital organs of wild Brevoortia patronus from the northern Gulf of Mexico after the Deepwater Horizon oil spill. *Ecotoxicology*, *24*(9), 1831.

Mordukhovich I, et al. (2010). Associations between polycyclic aromatic hydrocarbon-related exposures and P53 mutations in breast tumors. *Environmental Health Perspectives*, *118*(4), 511–518.

Nadler, A. M., & Bentivegna, C. S. (2017). *Effects of Crude Oil on Tumor Suppressor P53 Polymorphisms in Laboratory-Exposed Killifish*. PowerPoint.

Nomura, T., Kamada, R., Ito, I., Sakamoto, K., Chuman, Y., Ishimori, K., … Sakaguchi, K. (2011). Probing phenylalanine environments in oligomeric structures with pentafluorophenylalanine and cyclohexylalanine. Biopolymers, 95(6), 410–419. https://doi.org/10.1002/bip.21594

Oleksiak, M. F. (2008). Changes in gene expression due to chronic exposure to environmental pollutants. *Aquatic Toxicology*, *90*(3), 161–171.

Olivares-Rubio, H. F., et al. (2018). Lipid metabolism and pro-oxidant/antioxidant balance of Halamphora oceanica from the Gulf of Mexico exposed to water accommodated fraction of Maya crude oil. *Ecotoxicology and Environmental Safety*, *147*, 840–851.

Olson, G. M., Meyer, B. M., & Portier, R. J. (2016). Assessment of the toxic potential of polycyclic aromatic hydrocarbons (PAHs) affecting Gulf menhaden (Brevoortia patronus) harvested from waters impacted by the BP Deepwater Horizon Spill. Chemosphere, 145, 322–328.

Ozhan, K., Parsons, M. L., & Bargu, S. (2014). How Were Phytoplankton Affected by the Deepwater Horizon Oil Spill? *BioScience*, *64*(9), 829–836.

Passow, U., & Ziervogel, K. (2016). Marine Snow Sedimented Oil Released During the Deepwater Horizon Spill. Oceanography, 29(3), 118.

Piasecka, A., Brzuzan, P., Woźny, M., Ciesielski, S., & Kaczmarczyk, D. (2015). Splice-acceptor site mutation in p53 gene of hu888 zebrafish line. Journal of Applied Genetics, 56(1), 115–121.

Pongpiachan, S. (2014). Application of Binary Diagnostic Ratios of Polycyclic Aromatic Hydrocarbons for Identification of Tsunami 2004 Backwash Sediments in Khao Lak, Thailand.

Pongpiachan, S., et al. (2017). Assessing human exposure to PM10-bound polycyclic aromatic hydrocarbons during fireworks displays. *Atmospheric Pollution Research*, *8*(5), 816–827.

Ramesh, A., et al. (2004). Bioavailability and Risk Assessment of Orally Ingested Polycyclic Aromatic Hydrocarbons. *International Journal of Toxicology (Taylor & Francis)*, *23*(5), 301–333.

Reid, N. M., et al. (2017). The Landscape of Extreme Genomic Variation in the Highly Adaptable Atlantic Killifish. *Genome Biology and Evolution*, *9*(3), 659–676.

Retzlaff, M., Rohrberg, J., Küpper, N. J., Lagleder, S., Bepperling, A., Manzenrieder, F., … Buchner, J. (2013). The Regulatory Domain Stabilizes the p53 Tetramer by Intersubunit Contacts with the DNA Binding Domain. Journal of Molecular Biology, 425(1), 144–155. https://doi.org/10.1016/j.jmb.2012.10.015

Ren, H., et al. (2010). Continuous surface seawater surveillance on poly aromatic hydrocarbons (PAHs) and mutagenicity of East and South China Seas. *Estuarine, Coastal and Shelf Science*, *86*(3), 395–400.

Roth, J., Koch, P., Contente, A., & Dobbelstein, M. (2000). Tumor-derived mutations within the DNA-binding domain of p53 that phenotypically resemble the deletion of the proline-rich domain. Oncogene, 19(14), 1834–1842.

Rust, A. J., Burgess, R. M., McElroy, A. E., Cantwell, M. G., & Brownawell, B. J. (2004). Influence of Soot Carbon on the Bioaccumulation of Sediment-Bound Polycyclic Aromatic Hydrocarbons

by Marine Benthic Invertebrates: An Interspecies Comparison. *Environmental Toxicology & Chemistry*, *23*(11), 2594.
Saha, T., Kar, R. K., & Sa, G. (2015). Structural and sequential context of p53: A review of experimental and theoretical evidence. Progress in Biophysics and Molecular Biology, 117(2), 250–263.
Saranjampour, P., Vebrosky, E. N., & Armbrust, K. L. (2017). Salinity impacts on water solubility and n-octanol/water partition coefficients of selected pesticides and oil constituents. Environmental Toxicology & Chemistry, 36(9), 2274.
Schaefer, K. N., Geil, W. M., Sweredoski, M. J., Moradian, A., Hess, S., & Barton, J. K. (2015). Oxidation of p53 through DNA Charge Transport Involves a Network of Disulfides within the DNA-Binding Domain. Biochemistry, 54(3), 932–941. https://doi.org/10.1021/bi501424v
Schlereth, K., Heyl, C., Krampitz, A.-M., Mernberger, M., Finkernagel, F., Scharfe, M., … Stiewe, T. (2013). Characterization of the p53 Cistrome – DNA Binding Cooperativity Dissects p53's Tumor Suppressor Functions. PLoS Genetics, 9(8), 1–15.
SETAC. (1995). *The Mult-Media Fate Model: A Vital tool for Predicting the Fate of Chemicals*. USA: SETAC Press. Print.
Schulte, P. M. (2014). What is environmental stress? Insights from fish living in a variable environment. Journal of Experimental Biology, 217(1), 23–34.
Shukla, B., & Koshi, M. (2012). Importance of Fundamental sp, sp2, and sp3 Hydrocarbon Radicals in the Growth of Polycyclic Aromatic Hydrocarbons. *Analytical Chemistry*, *84*(11), 5007–5016.
Singleton, B., et al. (2016). Environmental stress in the Gulf of Mexico and its potential impact on public health. *Environmental Research*, *146*, 108–115.
Song, F., & Gao, Y. (2009). Chemical characteristics of precipitation at metropolitan Newark in the US East Coast. *Atmospheric Environment*, *43*(32), 4903–4913.
Sunnucks, P., Wilson, A. C., Beheregaray, L. B., Zenger, K., French, J., & Taylor, A. C. (2000). SSCP is not so difficult: the application and utility of single-stranded conformation polymorphism in evolutionary biology and molecular ecology. Molecular Ecology, 9(11), 1699–1710.
SYBR Gold Nucleic Acid Gel Stain (10,000X Concentrate in DMSO) - Thermo Fisher Scientific. (2018). Retrieved April 20, 2018.
Stimulation of microbial nitrogen cycling in aquatic ecosystems by benthic macrofauna: Mechanisms and environmental implications. (2013). Retrieved February 8, 2018
Turner, R. E. (2017). Smaller size-at-age menhaden with coastal warming and fishing intensity. Geo: Geography and Environment, 4(2), e00044.
Uversky, V. N. (2016). p53 Proteoforms and Intrinsic Disorder: An Illustration of the Protein Structure-Function Continuum Concept. *International Journal of Molecular Sciences*, *17*(11), 1–37.
Van Drooge, B. L., Marqueño, A., Grimalt, J. O., Fernández, P., & Porte, C. (2017). Comparative toxicity and endocrine disruption potential of urban and rural atmospheric organic PM 1 in JEG-3 human placental cells. Environmental Pollution, 230, 378–386.
Yang, M., Wu, J., Wu, S., Bi, A., & Liao, D. J. (2012). Splicing of mouse p53 pre-mRNA does not always follow the "first come, first served" principle and may be influenced by cisplatin treatment and serum starvation. Molecular Biology Reports; Dordrecht, 39(9), 9247–9256.
Yeo, C. Q. X., Alexander, I., Lin, Z., Lim, S., Aning, O. A., Kumar, R., … Cheok, C. F. (2016). p53 Maintains Genomic Stability by Preventing Interference between Transcription and Replication. Cell Reports, 15(1), 132–146.

Zadlock, F. (2017). Transcriptome Approach for Identifying Potential Biomarkers for Endocrine Disruption due to Crude Oil Exposure using Killifish (Fundulus Heteroclitus). Seton Hall University Dissertations and Theses (ETDs).